Molecular diffusion of mass and energy predicted by *ab initio* potential energy surfaces for air components at high temperatures

Paolo Valentini, Maninder S. Grover, and Nicholas J. Bisek

Phys. Rev. Fluids **9**, 013401 — Published 9 January 2024

DOI: 10.1103/PhysRevFluids.9.013401

Molecular diffusion of mass and energy predicted by *ab initio* potential energy surfaces for air components at high temperatures

Paolo Valentini* and Maninder S. Grover†
University of Dayton Research Institute, 1700 South Patterson Blvd, Dayton, OH 45469, USA

Nicholas J. Bisek‡
Air Force Research Laboratory, Wright-Patterson Air Force Base, OH 45433, USA
(Dated: December 19, 2023)

The thermal conductivity and self-diffusion coefficients for molecular nitrogen and oxygen are investigated with the direct molecular simulation (DMS) technique using high-fidelity, *ab initio* potential energy surfaces (PES). The DMS results are compared to available experimental data and remarkable agreement was observed in all cases. Such comparisons were restricted to relatively low temperature, typically below 2,000 K. For temperatures up to 10,000 K, the DMS data are also in excellent agreement with the corresponding transport properties obtained using kinetic theory based on collision integrals evaluated with simplified, point-particle interatomic potentials. An analysis of the Eucken approximation shows that the Eucken correction factor is based upon reasonably accurate assumptions, but a significant improvement can be obtained by properly accounting for the ratio of mass to momentum diffusion. Finally, it is shown that the DMS transport data for mass, momentum, and energy are consistent with kinetic theory across a wide range of temperatures, thus offering convincing evidence for the reliability of the methodologies employed for their determination.

I. INTRODUCTION

The accurate modeling of hypersonic flows represents a challenge due to the complex coupling between various physical and chemical phenomena that are the results of molecular-level interactions between the gas particles [1]. Depending on Mach number, the gas may be locally in a state of thermochemical nonequilibrium, caused by the high temperatures reached in the shock layer and the very fast flow speed. Such conditions are clearly very difficult or impossible to reproduce under controlled laboratory conditions. Therefore, in the past decade, there has been a significant effort to improve air thermophysical models using theoretical and computational approaches that hinge on *ab initio* potential energy surfaces (PESs) constructed using sophisticated quantum mechanical methods [2–10]. These PESs accurately describe the interaction between air components, both molecular and atomic. For this reason, they have been used in various molecular dynamics studies to investigate internal energy relaxation and chemical reactivity [3, 11–14], transport coefficients [15–17], and canonical one- and two-dimensional flows [18–21]. In some cases, reduced-order models have been informed using these analyses [22, 23].

Accurate characterization of transport coefficients is similarly affected by difficulties to reach very high temperatures within controlled experimental setups (usually up to about 2,000 K [24–27]). Furthermore, the uncertainty on the experimental measurements becomes larger and larger as temperature is increased [28]. For these reasons, the extrapolation of simple fitting functions from low to high temperatures is susceptible to large errors.

At typical hypersonic conditions, the laminar boundary layer is characterized by very strong temperature gradients, due to the relatively cold wall with respect to the hot shock layer, and by species mole fraction gradients, due to chemical reactivity triggered by the post-shock conditions [29]. These gradients force diffusion mechanisms that transport both energy and mass across the boundary layer. Such phenomena, in turn, affect the heat flux at the wall and, in the presence of surface-mediated chemistry, may augment the total surface heat flux and affect the surface chemical composition. Hence, the precise description of these mechanisms is important in the design of hypersonic aeroshells, particularly when reusability becomes a constraint.

Transport collision integrals used in computational fluid dynamics (CFD) [30, 31] were generally obtained from kinetic theory using semi-empirical, simplified molecular interaction models [32, 33], many dating back several decades ago. Although not necessarily inaccurate, such interatomic potentials were too simplistic to realistically model atom-diatom and diatom-diatom interactions. For these reasons, the use of *ab initio* PESs to characterize transport properties is valuable to further refine or verify these semi-empirical collision integrals.

For more complex molecular interaction potentials for which transport integrals cannot be evaluated by a simple, one-dimensional numerical integration [34], the quasi-classical trajectory (QCT) method [35] has been used to obtain the collision integrals via Monte Carlo quadrature. However, for systems characterized by a high dimensionality of the reactants' configuration space, e.g., diatom-diatom collisions, several simplifying assumptions to reduce the sampling space must be made in order

* Senior Aerothermodynamic Research Engineer, University of Dayton Research Institute, Dayton, OH; pvalentini1@udayton.edu
† Aerothermal Research Engineer, University of Dayton Research Institute, Dayton, OH; mgrover1@udayton.edu
‡ Senior Research Aerospace Engineer, AFRL/RQHA, 2210 Eighth Street, Wright-Patterson AFB, OH; nicholas.bisek.1@us.af.mil

to keep the problem computationally tractable. For example, Mankodi *et al.* [17] have recently presented QCT-obtained data for shear viscosity of molecular nitrogen and oxygen. In their QCT calculations, however, they consider reactant molecules in the ground rotational state only and having different vibrational states. Subramaiam *et al.* [36] compute transport collision integrals for $O+O_2$ using *ab initio* PESs. In their work, the orientation of the O_2 molecule is assumed to be fixed and the one-dimensional collisional relations for scattering angle, cross-section, and collision integral [34] are considered for different vibrational levels obtained for a rotation-less molecule. Although some of these assumptions have been shown to be adequate with comparisons to DMS [15], they cannot be assumed to have general validity.

Recently, we have used the direct molecular simulation (DMS) method [37] to investigate transport coefficients for air components at high temperature. The DMS method is essentially a first-principles variation of the direct simulation Monte Carlo (DSMC) method [38]. In fact, the simplified, often phenomenological, collision models used in DSMC are all replaced by molecular dynamics trajectories on a PES. In essence, DMS embeds trajectory calculations within a time accurate flow simulation where, like DSMC, particle collisions occur stochastically and are decoupled from particle advection. In a previous study, we used the DMS method to obtain shear viscosity data for air components up to 10,000 K [15]. These predictions were obtained by only using first-principles PESs. The results compared favorably with both experimental and QCT data [17].

The current study presents an investigation on molecular diffusion of energy and mass for air components at high temperature. All predictions are obtained from *ab initio* potentials. In particular, we focus on thermal conductivity and its connection to mass diffusion at the molecular scale. Recently, we have described a relatively simple and efficient computational technique applicable to the DMS method to estimate thermal conductivity from *ab initio* PESs [16]. Here, we present a refinement and extension of our previous results [16] that were restricted to molecular nitrogen only. In addition to obtaining thermal conductivity predictions for molecular oxygen and non-reactive air, we investigate the commonly used Eucken correction [34] by determining self-diffusion coefficients for pure components, once again only relying on the *ab initio* PESs. With this comprehensive analysis, we show how the DMS data for all transport properties are consistent with well-established kinetic theory results. This demonstrates the validity of the proposed *ab initio* methodologies.

This article is organized as follows: In Sec. II, we outline the DMS numerical technique (Sec. II A) and the PESs that were utilized in the computations (Sec. II B). For clarity, we detail the basic features of the *modified* Müller-Plathe (MMP) method in Sec. II C, which we presented in detail in a previous study on thermal conductivity [16]. Then, the approach to obtain self-diffusion mass transport coefficient is described in Sec.II D. The results are presented and discussed in Sec. III with comparisons to well-established experimental data and other theoretical and computational results. An analysis of the Eucken correction is presented in Sec. III C. Finally, the conclusions are summarized in Sec. IV.

II. NUMERICAL METHOD

A. Direct Molecular Simulation

The DMS method has been extensively presented in several previous references [11–14, 18, 37, 39], but a brief summary will be provided here. As stated, the DMS technique is based on the same formulation as DSMC, with the exception of the mapping from reactant to product states. In DSMC, this mapping is efficiently achieved with analytic functions of a set of pre-collision quantities (e.g., total collision energy, impact parameter, initial states). These functions do not necessarily reproduce microscopic collision outcomes accurately, but recover macroscopic relations. For example, the variable hard sphere model (VHS) accurately reproduces the viscosity cross-section, but for each collision, the scattering angle is simply randomized. For these reasons, such models are often referred to as phenomenological. In DMS instead, each collision is tracked with high fidelity by a molecular dynamics trajectory that deterministically maps the initial states to the final states. Importantly, because collisions occur on *ab initio* PESs that do not contain any empiricism, the resulting macroscopic predictions for transport phenomena are only the result of the molecular-level interactions that are derived from quantum mechanics only.

Like DSMC, DMS simulations are carried out using time steps of the order of the smallest mean collision time in the flow,the cell sizes in the flow field are of the order of the local mean free path, and, by using a particle weight, only a subset of real particles in each control volume is simulated and collided. The no time counter (NTC) algorithm [38] is used to select particle pairs for collisions in each cell [37]. A sufficiently large hard-sphere total cross-section $\sigma = \pi b_{max}^2$ based upon the maximum impact parameter b_{max} is used to conservatively ensure that all collisions having a non-negligible angle of deflection are simulated. This is particularly important for transport coefficients since they are functions of integrals of the scattering angle over all impact parameters [34].

DMS particles possess all the internal phase-space coordinates needed to describe their structure (e.g., single atoms, diatomics, triatomics, etc.). When selected for trajectory integration, their coordinates are propagated in time by integrating Newton's second law of motion with a time step of the order of 1 fs. Trajectories are truncated when the products are separated by a distance D_0, which is set large enough that no further state changes are possible. All molecular state transitions, solely governed by the PES and compatible with the local gas thermodynamic state, are permitted. DMS is therefore governed by all the well-known underlying dilute gas assumptions of DSMC (e.g., binary collisions, molecular chaos, etc.) but, remarkably, its overall

TABLE I. *Ab initio* potential energy surfaces

Interaction	Reference(s)
N_2+N_2	Bender *et al.*[2, 3]
O_2+O_2	Paukku *et al.* (singlet and quintet) [4] Paukku *et al.* (triplet) [5]
N_2+O_2	Varga *et al.*[8]

accuracy is entirely traceable to the PES, which is the only molecular modeling input. The high fidelity nature of the method is reflected in its significant computational cost, primarily due to the integration of millions or billions of molecular trajectories on *ab initio* PESs.

B. Potential energy surfaces

Molecular interactions were modeled with *ab initio* PESs. All PESs are listed in Table I for each interaction together with the references containing the computational details of the quantum mechanical methods [2–5, 8]. For N_2+N_2 and N_2+O_2 collisions, trajectories are integrated on the respective PESs. However, for molecular oxygen collisions, trajectories occur on one of three surfaces (Table I), with probability 1/9 (singlet), 3/9 (triplet) and 5/9 (quintet). No electronic excitation is considered in this work as only ground-state PESs for O_2+O_2 collisions were available as of the writing of this article. However, the method presented here is not inherently restricted to adiabatic dynamics, and once PESs for electronically excited states are produced, the effect of electronic excitation could be investigated by including non-adiabatic trajectories. Moreover, accurate collision-specific, ground-state cross-sections for neutrals are still needed in kinetic particle methods (e.g., DSMC) for the simulation of hypersonic flows in thermochemical nonequilibrium [40] or plasmas [31].

In all simulations presented here, we set the maximum impact parameter b_{max} for collisions to 6 Å and interactions are cut off when reaction products are separated by a distance of at least $D_0 = 20$ Å. Trajectories are integrated using the velocity-Verlet algorithm [41] with a fixed time step, set between 0.05 fs and 1 fs, with the smaller values used at the higher temperatures. A thorough discussion on the proper choice of DMS simulation parameters is contained in previous works [19, 37].

C. Thermal conductivity coefficient and simulation setup

In Ref. [16], we proposed and tested a methodology to compute the coefficient of thermal conductivity for a dilute gas using DSMC, DMS, or other particle methods. The approach was inspired by the classic Müller-Plathe technique [42], in that the heat flux is imposed on the system and, consequently, it is precisely known. The resulting temperature gradient is instead sampled during the simulation. In this manner, the issue of large statistical scatter associated with sampling the heat flux in Fourier flows is overcome. For these reasons, we named the method *modified* Müller-Plathe [16]. The MMP approach is particularly advantageous when applied to *ab initio* DMS, which is based on PESs that are computationally expensive.

To summarize the MMP method for clarity, we start with the simple Fourier relation:

$$\mathbf{J} = -\kappa(T)\nabla T, \tag{1}$$

where $\mathbf{J}$ is the heat flux vector which causes the temperature gradient ∇T. In Eq. 1, the thermal conductivity κ is taken as a scalar quantity, a reasonable assumption for isotropic dilute gases. Because of its temperature dependence, κ should be rigorously computed from a heat flux in the limit of a vanishing temperature gradient. For simplicity, we assume that the heat flux is in the x-direction, J_x, and, therefore, the limit $\partial T/\partial x \to 0$ should hold:

$$\kappa(T) = \frac{-J_x}{\partial T/\partial x}. \tag{2}$$

Similar to the MP method, in the MMP approach, the simulation box is subdivided into n_s slabs of equal width Δx along the x-direction. At $x = 0$ and $x = L$, isothermal wall boundary conditions are imposed at T_w, and, for simplicity, $T_w(0) = T_w(L) = T$. Periodicity is used in the y and z directions. At each DMS time step Δt, particles located in the middle slab, i.e., whose $x \in [L/2 - \Delta x/2, L/2 + \Delta x/2]$ are given additional center of mass kinetic energy $\delta\varepsilon$ with a probability p_ε. If selected for the energy *kick*, the particle new center of mass velocity vector magnitude $|\mathbf{v}_{new}|$ is corrected as

$$|\mathbf{v}_{new}| = \sqrt{\mathbf{v}_{old}\cdot\mathbf{v}_{old} + 2\frac{\delta\varepsilon}{m}}, \tag{3}$$

where $\mathbf{v}_{old}$ is the old center-of-mass velocity vector and m is the particle mass. Then, the new center-of-mass velocity vector direction is assigned from a uniform distribution on a unit-radius sphere. In this way, the heat flux imposed on the system is given by:

$$J_x = \frac{1}{2}\frac{p_\varepsilon N_{1/2}\delta\varepsilon W_p}{A\Delta t}, \tag{4}$$

where $N_{1/2}$ is the number of particles contained in the central slab, W_p is the particle weight, and A the cross sectional area of the simulation domain perpendicular to the x axis. The factor $\frac{1}{2}$ accounts for the propagation of the energy added to the system in both x directions. This energy addition produces an energy flux from the middle of the simulation box to the isothermal walls, with a temperature gradient established between the middle of the simulation box and the walls.

Often, it is convenient to decompose the thermal conductivity coefficient as

$$\kappa = \kappa_t + \kappa_{int}, \tag{5}$$

where κ_t and κ_{int} account for translational and internal energy transport, respectively. For diatomic molecules, κ_{int} accounts for rotational and vibrational modes. Whereas the rotation-translation energy transfer is generally very rapid, vibration-translation energy exchanges tend to be much slower, more so at temperatures below the temperature corresponding to the zero-point energy $\theta_v/2$, where θ_v is the characteristic vibrational temperature (2256 K for O_2 and 3371 K for N_2 [43]). Therefore, at low temperature, Eq. 1 should be rewritten as [34]:

$$\mathbf{J} = -\kappa_t\nabla T_t - \kappa_{int}\nabla T_{int}, \tag{6}$$

where T_t and T_{int} represent the translational and internal temperatures, respectively. By construction, energy is added to the translational degrees of freedom (Eq. 3). Therefore, incomplete equilibration of T_t and T_{int} may persist in the simulation box at low temperatures. In particular, at the lowest temperatures considered here, there is negligible excitation of vibrational degrees of freedom, i.e., $\partial T_v/\partial x \simeq 0$, where T_v represents the vibrational temperature. For this reason, we have excluded the contribution of vibrational degrees of freedom from Eq. 2 for translational temperatures well below or near θ_v. Therefore, Eq. 6 is rewritten as

$$\mathbf{J} \simeq -\kappa_{tr}\nabla T_{tr}, \tag{7}$$

where T_{tr} denotes the rotranslational temperature and κ_{tr} only contains the contribution from translational and rotational modes. At high temperatures, however, no such simplification is needed, as the vibrational temperature is equilibrated with both the translational and rotational temperatures. An estimate of the error associated with ignoring the energy content in vibrational degrees of freedom was done in Ref. [16] by comparing variable hard sphere (VHS) DSMC solutions with a temperature-dependent vibrational relaxation number model [38]. The resulting thermal conductivity coefficient at 273 K with only partial vibrational equilibration was about 15% lower than the value corresponding to full equilibration of internal energy modes. At 2,000 K, the difference dropped to only about 4%. At even higher temperatures, the error was found to becomes vanishingly small because the heat flow time scale becomes comparable to that of vibrational relaxation, as discussed earlier.

Finally, we point out that quantum mechanics forbids real gas molecules from possessing a vibrational energy below the so-called zero-point energy. Hence, for temperatures $T < \theta_v/2$, the internal heat capacity of the gas $c_{v,int}$ should mostly account for the rotational degrees of freedom. As discussed in Appendix A of Ref. [44], at thermal equilibrium conditions, the thermal conductivity coefficient also includes contributions from electronic excitation and free electrons. The PESs used in this work only describe ground states (Sec. II B) and no free electrons are modeled. Therefore, these contributions are not included in Eq. 6. In the following, we will simply refer to the total thermal conductivity as κ.

The simulation box consisted of 250 cubic cells aligned along the x axis, for a total length of 10 μm, while periodicity was used in the y and z directions. A total of 21,000 particles were used, with approximately 80 simulator particles contained in each cell, whose side was set to about 0.9λ, where λ is the local mean free path estimated with the VHS model with parameters consistent with the gas viscosity [15]. A conservative time step of 5 ps was used in the simulations and the particle weight W_p was set to 10^9, corresponding to a mass density around 2 kg/m^3. The number of *slabs* used was 50. The kinetic energy added per particle was varied to obtain a relatively small temperature variation across the channel. The Knudsen number based on the channel width is estimated to be around 10^{-3}, hence a negligible temperature jump is found at the walls. For all calculations, we set $p_\varepsilon = 0.01$.

Particle collisions with the wall were modeled as fully diffuse. Molecules were scattered with a new center-of-mass velocity vector, sampled from a Gaussian distribution consistent with the surface temperature. Both walls were maintained at the same temperature. Similarly, the internal phase-space coordinates were assigned to correspond to internal energies (rotational and vibrational) distributed according to a Boltzmann distribution at the wall temperature, without any correlation with the internal states prior to the collision with the wall. The vibrational states of the wall-scattered molecules were assigned using fractional

vibrational states for each of the allowed rotational states, using the Wentzel-Kramers–Brillouin (WKB or quasi-classical) approximation [35]. Specifically, 20 vibrational sub-levels were used to fill the gap between the energy levels corresponding to integer vibrational numbers at a given rotational level. Because molecules in the interior of the simulation domain can occupy a continuum of states, from the bottom of the diatomic potential to the dissociation threshold, no zero-point energy constraint was imposed in the generation of states for wall-reflected molecules. Importantly, the walls simply imposed complete thermal and velocity accommodation, resulting in a near no-slip wall boundary condition. This enables a comparison with the analogous continuous heat flow described by the Fourier law. Therefore, the transport data presented here should be interpreted as consistent with the Chapman-Enskog approximation.

The initial chemical composition was maintained by ignoring all simple and double dissociations. The phase-space coordinates were reset to their initial pre-collision values whenever a molecule underwent dissociation. Exchange reactions, which do not change the chemical composition for single species systems, were permitted instead. However, for N_2+O_2, exchange processes were ignored in the same manner as dissociations (i.e., non-reactive air).

Figure 1 shows an example of temperature profiles in pure O_2 obtained while sampling at steady state for wall temperatures of 2,000 K and 8,000 K. The temperature gradient causes a modest density variation across the channel. As shown in Fig. 1a, at a temperature near or below the characteristic vibrational temperature (2256 K for oxygen), the temperature associated with internal modes T_{int} corresponding to the internal energy is only partially equilibrated with the translational temperature. This is primarily due to the slow transfer of energy from external to vibrational degrees of freedom. At 8,000 K, however, vibration-translation energy exchange becomes much faster and leads to full thermal equilibration, as shown in Fig. 1b.

The temperature gradient used to evaluate κ is obtained from the average of linear fits of the temperature profiles at $x/L \in [0, 0.1]$ and $x/L \in [0.9, 1]$, where the gas temperature is closer to the nominal value at which $\kappa(T)$ is estimated. This, with the exceptions of cases at near ambient temperature, also mitigates the issues associated with incomplete equilibration of T_{int}, as discussed later. Samples were collected for a minimum of 500,000 time steps after the system had reached steady state. Profiles were averaged over 10,000 steps at steady state and the uncertainty on κ was given using a standard error of the mean based upon collecting 10 to 20 samples.

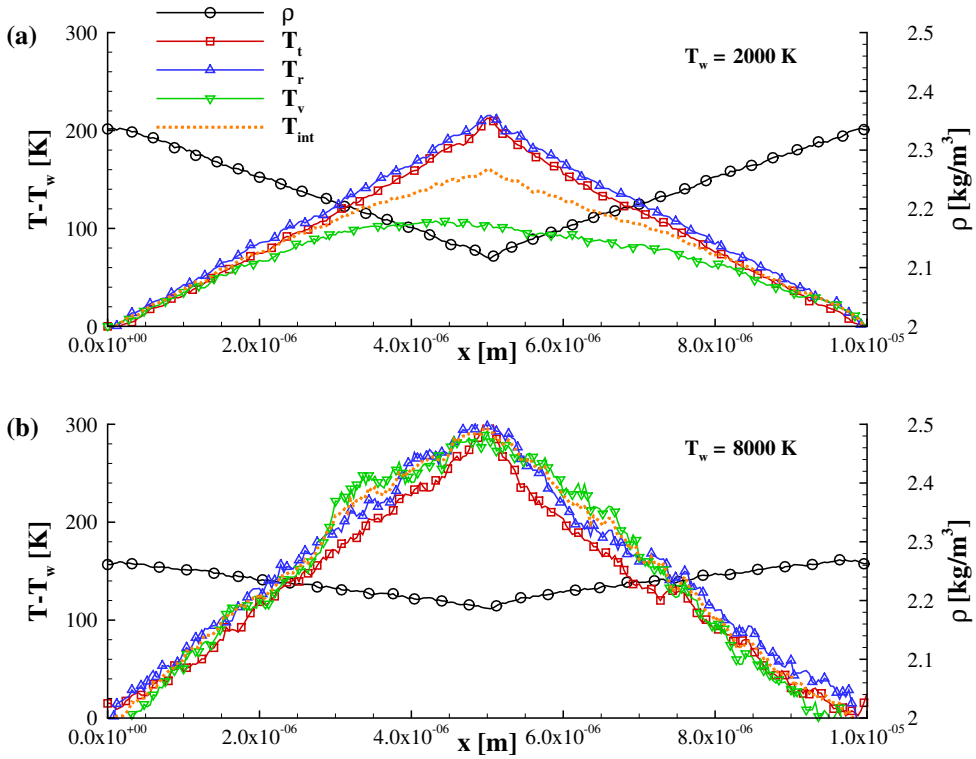

FIG. 1. Temperature gradients obtained by imposing a heat flux via Eq. 4 and corresponding density variations across the channel for pure molecular oxygen (a) at 2,000 K and (b) at 8,000 K.

D. Self-diffusion coefficient and simulation setup

The self-diffusion coefficient can be envisioned as the diffusion of one isotopic gas into another isotopic form of the same gas. Clearly, in the case of physically indistinguishable particles, only the theoretical definition can be applied, as its experimental determination would not be possible. Instead, in our simulations, identical molecules can be *computationally tagged* with different labels. Such labels have no effect on molecular interactions, which are solely derived from the PESs. This enables us to track the diffusion of chemically identical, but differently tagged, molecules.

To compute the self-diffusion coefficient, the simulation box was initialized with a mole fraction discontinuity at $L/2$. In practice, the box contained only molecules labeled α for $x < L/2$ and labeled β for $x > L/2$. Along the x axis, the domain contained 10,000 cubic cells, for a total length of 50 μm. Periodicity was used in the y and z directions. The number density was set to 4.2×10^{25} m^{-3}, corresponding to a mass density of about 2 kg/m^3. To obtain a minimum of 80 simulator particles in each cell, a particle weight of 1.25×10^9 was imposed, thus resulting in approximately 800,000 total simulated molecules. The local mean free path λ was greater than three times the cell size for all cases. A conservative time step of 1.25 ps was used to integrate particle advection. Particle collisions with the walls at $x = 0$ and $x = L$ were modeled as specular. Finally, the initial chemical composition was maintained in the same manner described for the thermal conductivity calculations.

Note that the system is initialized with a uniform temperature across the channel. Therefore, the only driving force for mass diffusion is the mole fraction gradient. As shown in Fig. 2, as time progresses, the system tends to evolve toward $\chi = \frac{1}{2}$, as expected by the integration of the simple diffusion equation

$$\frac{\partial \chi}{\partial t} = D \frac{\partial^2 \chi}{\partial x^2}, \tag{8}$$

which admits a simple analytic solution corresponding to the Heavyside initial condition described earlier and uniform far-field boundary conditions [45]:

$$\chi_{\alpha,\beta} = \frac{1}{2} \mp \frac{1}{2} \operatorname{erf}\Big(\frac{x - L/2}{\sqrt{4Dt}} \Big). \tag{9}$$

The DMS profiles, like those shown in Fig. 2(a) for a system at 8,000 K, are then fit using Eq. 9 by a least-square procedure to obtain D. Note that $D_{\alpha\beta} = D_{\beta\alpha} = D$ and, therefore, two set of profiles per each time t are fit to obtain χ_α and χ_β. The corresponding diffusion coefficients D are then averaged to improve the statistics.

Mole fractions profiles were extracted at regular intervals of 1.25 ns, as shown in Fig. 2(b). After an initial transient, D remains approximately constant, so long as the *far* boundaries are not reached. Self-diffusion coefficients extracted in the sampling window are then averaged. A statistical uncertainty is assigned assuming a confidence interval of 95% and was generally found to be less than 3%. Finally, the procedure was repeated for various equilibrium temperatures.

III. RESULTS AND DISCUSSION

A. Thermal conductivity coefficients

DMS predictions for the thermal conductivity coefficent were obtained for molecular nitrogen and oxygen, and their mixture using mole fractions of 22% and 78% for O_2 and N_2, respectively. In all cases, the reported DMS data have an uncertainty of less than 5% assuming a confidence interval of 68%. As discussed previously, the finite temperature gradient introduces an error on the temperature T at which $\kappa(T)$ is evaluated. This error was conservatively set to the amplitude of the temperature variation across the channel and can be reduced by decreasing $\delta\varepsilon$ (Eq. 4). However, no confidence bounds can be established for this type of uncertainty.

All data are compared to the zero-density limit experimental correlation of Lemmon and Jacobsen [25]. This correlation was obtained by an extensive analysis of existing experimental data and was generally within 5-6% of the actual experimental data points. For this reason, we use it as a surrogate of the experimental measurements for ease of presentation. It is important to emphasize once again that experiments are limited to temperatures below about 2000 K, with the vast majority of them at near room temperature and pressure [25].

The DMS data are also compared with the thermal conductivity coefficient computed using the collision integrals for air species obtained from simplified potentials [30, 31]. It is worth mentioning that the collision integrals from Ref. [30] are recommended for use in popular computational fluid dynamics (CFD) solvers for hypersonic flows, including the Data Parallel Line Relaxation (DPLR) [46] CFD code.

As shown in Figs. 3 to 5, the DMS predictions for κ are found to be in good accordance with the experimental data [25]. In the experimental temperature range of 273 K to 2,000 K, shown in Figs. 3a-5a, the average error between the DMS predictions and the empirical correlation is about 9%. As discussed in Ref. [16], this discrepancy (which reaches about 20% at 273 K for all gas

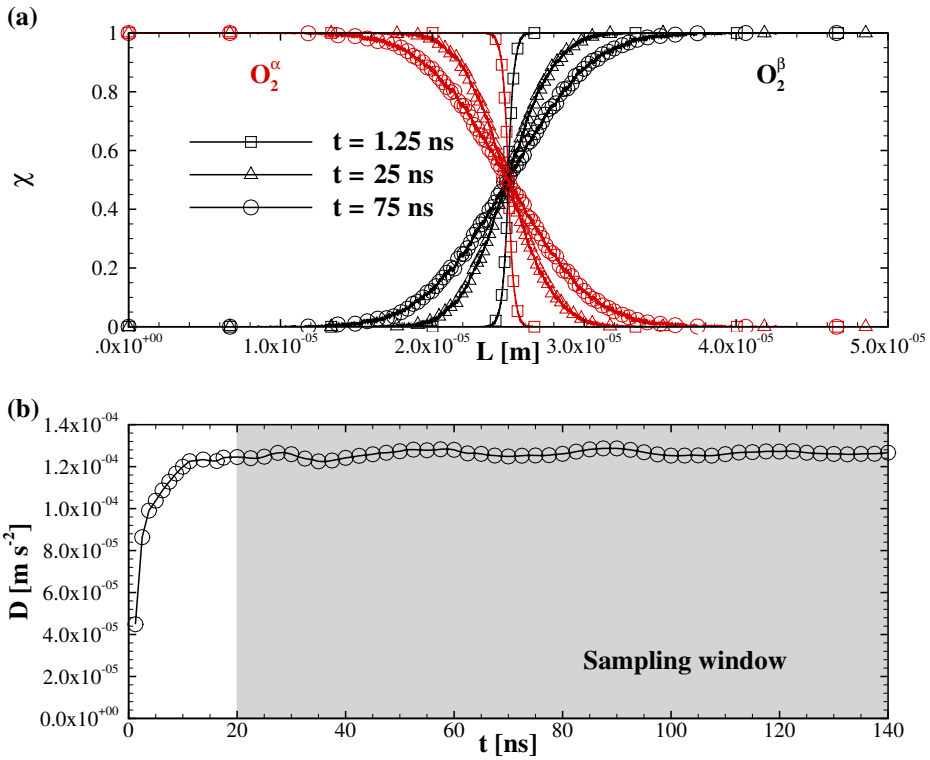

FIG. 2. (a) Evolution of mole fractions for pure molecular oxygen at 8,000 K. O_2^α and O_2^β are chemically identical, but have been assigned a different *computational label*. (b) Corresponding diffusion coefficient from least-square fit of transient profiles.

systems considered) may be attributed to only partial vibrational energy equilibration, as vibration-translation energy relaxation times are extremely long at near room temperatures. Furthermore, the PESs utilized in this work were developed with a focus on high-energy collisions, which are more representative of high-temperature gas environments [2]. Therefore, their performance at low temperature may be degraded [19, 21].

Over the wider temperature range (up to 10,000 K), the thermal conductivity coefficients obtained from collision integrals for molecular nitrogen and molecular oxygen agree well with the DMS data, as shown in Figs. 3b-5b. For N_2+N_2, the DMS predictions are slightly closer to the results of Capitelli *et al.* [31] than those of Wright *et al.* [30],whereas for molecular oxygen the three sets of data nearly overlap.

For mixtures, the heat flux is not only a function of the temperature gradient, but is affected by thermal diffusion and baro-diffusion [34, 47]. Hence, it is convenient to distinguish between *partial* (λ') and *true* (λ) coefficient of thermal conductivity [47], where λ' only accounts for the temperature gradient (Fourier relation) in the total heat flux. The coefficient λ instead also includes the contribution from thermal diffusion, via the thermal diffusion coefficient D_T [47]. For a stationary system, where diffusion velocities vanish, the difference $\lambda - \lambda'$ is of the order D_T^2 [47], and thus, it is generally assumed to be small. In the case of N_2+O_2 mixtures, because of the relatively similar molecular masses, we expect $\lambda - \lambda'$ to be negligible. However, neglecting the contribution from thermal diffusion may not be applicable to problems involving chemical species of significantly different molecular masses, for example in hydrogen combustion [48]. The results presented here are for a stationary gas mixture and are obtained by using Eq. 2, and thus are for the *true* coefficient of thermal conductivity [47]. DMS data on thermal diffusion for air-relevant binary mixtures will be presented in future work.

In Fig. 5, the DMS predictions for the total thermal conductivity coefficient for non-reactive air are compared to the kinetic theory data of Gupta *et al.* [44] for equilibrium air at 1 atm. The composition, which affects the overall thermal conductivity coefficient, is set to 22% O_2 and 78% N_2 by mole. As shown, the DMS and kinetic theory data very well at low temperatures (Fig. 5a). The agreement extends up to about 4,000 K, but a larger discrepancy can be observed at temperatures greater than about 6,000 K. This is expected as the assumption of an entirely molecular composition starts to break down. Nevertheless, the DMS data are still useful to calibrate collision-specific models or mixture rules, such as those used in DSMC or CFD.

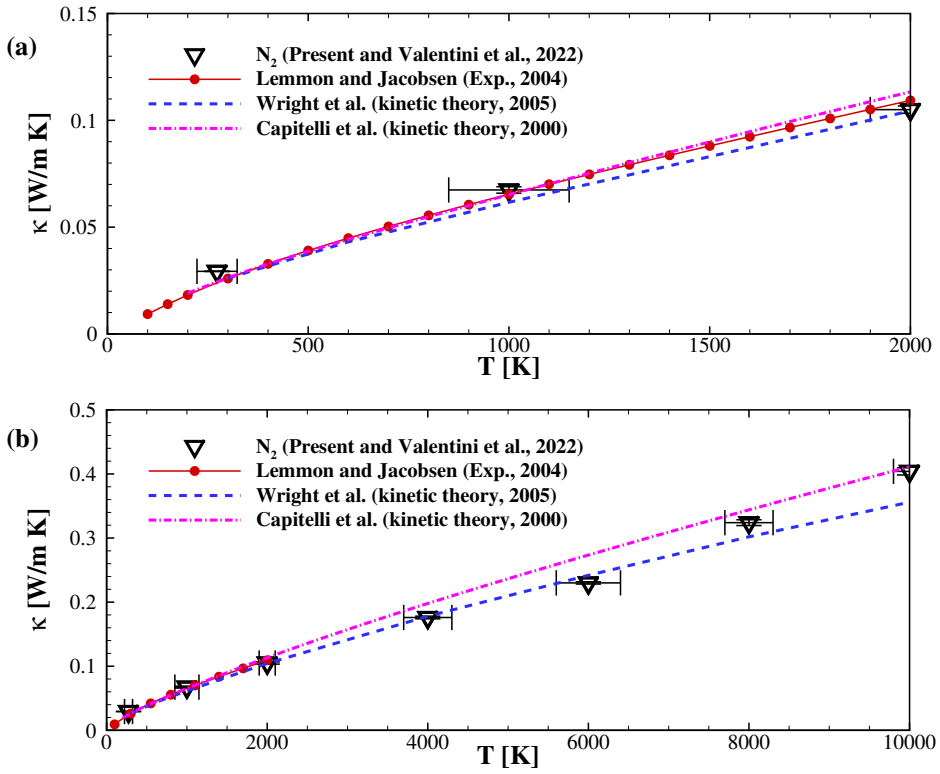

FIG. 3. Thermal conductivity of molecular nitrogen from DMS calculations using the MMP method. Comparison with the experimental data [25] and transport collision integrals models [30, 31].

A simple power law relation was used to fit the DMS data for the pure components:

$$\kappa(T) = \kappa_0 \left(\frac{T}{T_0}\right)^{\zeta}, \tag{10}$$

where the reference temperature T_0 is set to 273 K. Note that the power-law exponent ζ should not be taken as the viscosity index utilized, for example, in the VHS or variable soft sphere (VSS) DSMC models [38]. The fitting parameters are contained in Tab. II.

Interaction	κ_0 [W/m K]	ζ
N_2+N_2	0.0179	0.861
O_2+O_2	0.0239	0.805

TABLE II. Power-law fitting parameters for thermal conductivity coefficients of pure molecular nitrogen i and oxygen.

B. Self-diffusion coefficients

DMS predictions for the self-diffusion coefficient were obtained for pure molecular nitrogen and pure molecular oxygen. In all cases, the reported DMS data have an uncertainty of less than 3% assuming a confidence interval of 95%.

The experimental data for self-diffusion coefficients is scarce and, to our knowledge, limited to near room temperatures. As shown in Fig. 6, the DMS data obtained for molecular nitrogen agree quite well with the experimenal evidence of Winn [49] and Boardman *et al.* [50].

Over the temperature range considered in this work (up to 8,000 K), the self-diffusion coefficients obtained from collision integrals for molecular nitrogen and molecular oxygen agree very well with the DMS data, as shown in Figs. 7-8. For nitrogen, there is a near-exact agreement with the data of Wright *et al.* [30]. The results of Capitelli *et al.* [31] tend to overpredict the

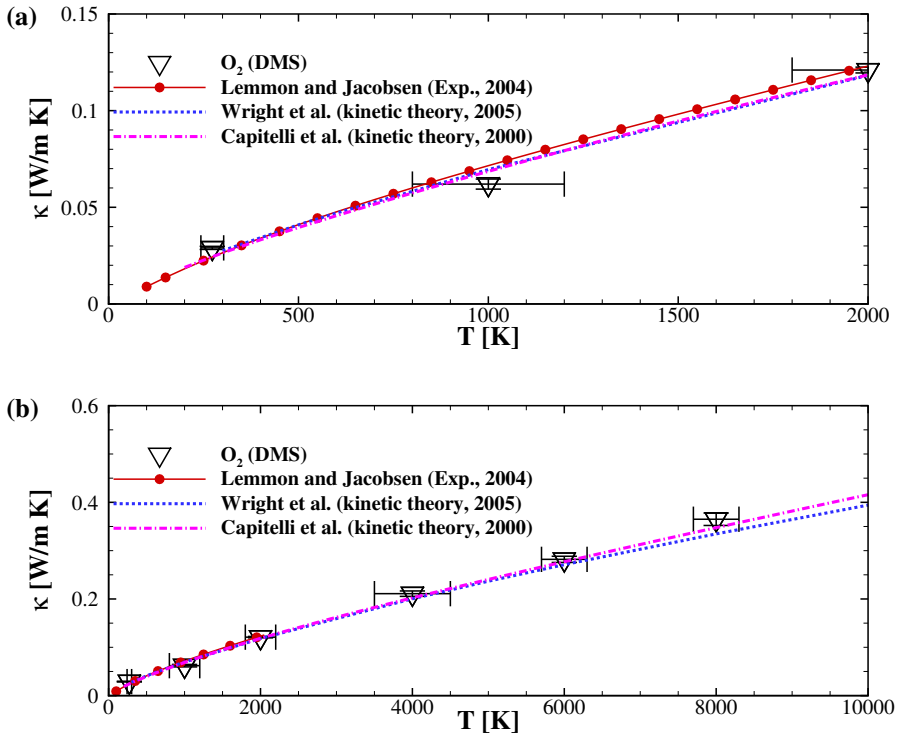

FIG. 4. Thermal conductivity of molecular oxygen from DMS calculations using the MMP method. Comparison with the experimental data [25] and transport collision integrals models [30, 31].

DMS data, particularly at the higher end of the temperature spectrum, up to about 15% at 8,000 K, as illustrated in Fig 7. At variance with nitrogen, all data sets agree remarkably well for molecular oxygen self-diffusion, as shown in Fig. 8. This level of agreement was also found for thermal conductivity coefficients in Sec. III A. The DMS data are also compared to the variable soft sphere (VSS) predictions based on the model parameters of Weaver and Alexeenko [51] for temperatures up to 2200 K. The VSS data underestimate the DMS and the collision integral data [30, 31] by up to 20%.

C. The Eucken approximation

For molecules possessing internal degrees of freedom, a typical approximation is to assume a correction to the thermal conductivity of gas as if it were monoatomic and to approximately treat the transfer of energy between external and internal modes. This approximation is known as Eucken correction [34]:

$$\kappa = \frac{15}{4}\frac{R_u}{M}\eta\left(\frac{4}{15}\frac{c_v}{R_u}+\frac{3}{5}\right), \tag{11}$$

where R_u is the universal gas constant, M is the molecular mass, c_v is the constant-volume heat capacity, and η the (first approximation) of the gas viscosity coefficient. Assuming a structureless gas, the thermal conductivity has only a contribution from the translational degrees of freedom, i.e.,

$$\kappa_t = \frac{15}{4}\frac{R_u}{M}\eta. \tag{12}$$

To assess the validity of Eq. 11, we computed κ_t using the viscosity data in Ref. [15], which were obtained from the same PESs used in this work and by using the same simulation technique. Specifically, we used a simple power-law dependence on temperature for shear viscosity [15]: For N_2+N_2 interactions:

$$\eta = \eta_0\left(\frac{T}{T_0}\right)^{\omega}, \tag{13}$$

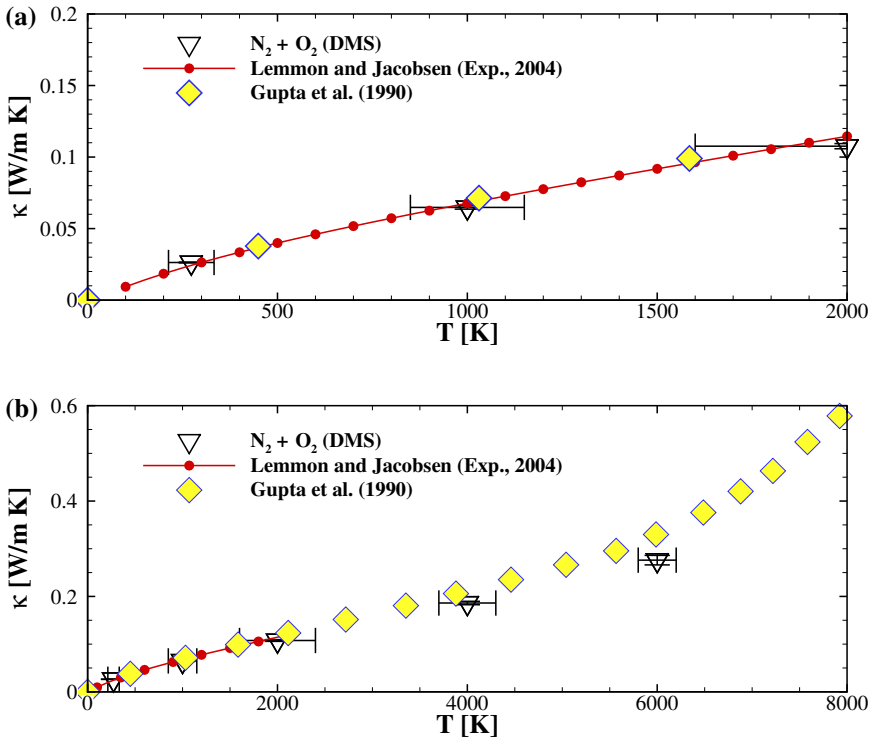

FIG. 5. Thermal conductivity for a mixture of 22% O_2 and 78% N_2 by mole fraction from DMS calculations using the MMP method. Comparison with the experimental data [25] and the kinetic theory result of Gupta *et al.* [44].

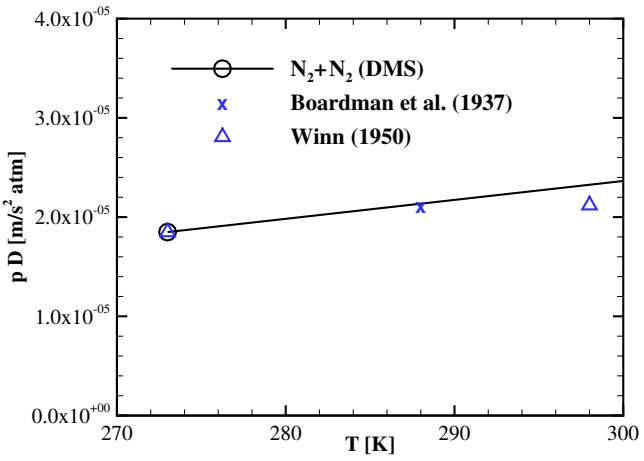

FIG. 6. Molecular nitrogen self-diffusion coefficient from DMS and comparison with experimental data [49, 50].

where $\eta_0 = 17.0\ \mu$Pa s and $\omega = 0.663$ for N_2+N_2 interactions and $\eta_0 = 20.2\ \mu$Pa s and $\omega = 0.662$ for O_2+O_2 interactions [15]. The reference temperature T_0 was set to 273 K.

Assuming a fully classical treatment of molecular motions, as is the case in our DMS calculations, we can write:

$$\frac{c_v}{R_u} = \left(\frac{3}{2}R_u + R_u + R_u\right)/R_u, \tag{14}$$

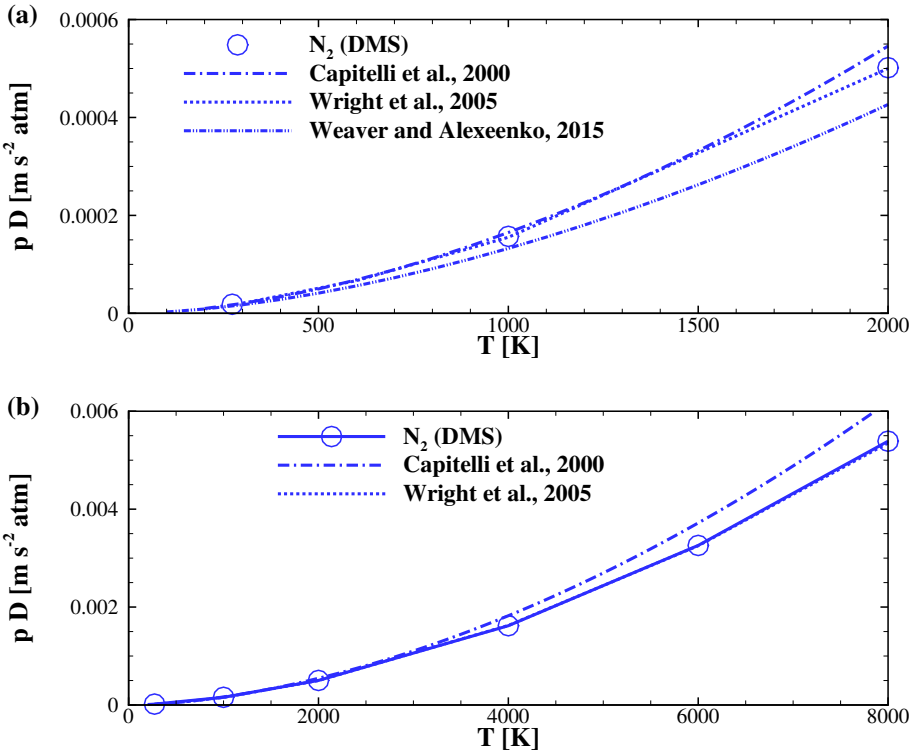

FIG. 7. Molecular nitrogen self-diffusion coefficients from DMS and from transport collision integrals [30, 31, 51]: comparison at (a) low temperature and (b) over the entire temperature range considered in this work.

where each contribution corresponds to translational ($\frac{3}{2}R_u$), rotational (R_u), and vibrational (R_u) degrees of freedom. The resulting expression for κ (Eq. 11) can then be simplified as

$$\kappa = \kappa_t(1+\frac{8}{15}). \tag{15}$$

We define the Eucken correction factor as

$$Eu = \kappa/\kappa_t, \tag{16}$$

where the total thermal conductivity κ was obtained from DMS.

As shown in Fig. 9a, the Eucken correction factor Eu that is obtained from DMS shows a relatively significant temperature dependence for both nitrogen and oxygen. However, it is close to the rough approximation in Eq. 15, i.e., 1+8/15. Importantly, Eq. 11 is obtained by making the further assumption that $\rho D/\eta = 1$, where D is self-diffusion coefficient [34]. The ratio of mass to momentum diffusion obtained from DMS was found to be about 20% to 50% larger than $\rho D/\eta = 1$, as shown in Fig. 9b. Further refinements to the Eucken correction have also been proposed to better reproduce the experimental data [52].

The more general relation, obtained from kinetic theory, reads instead [34]:

$$\kappa = \frac{1}{4}\Big[\big(15-6\frac{\rho D}{\eta}\big)\gamma-\big(15-10\frac{\rho D}{\eta}\big)\Big]c_v\eta, \tag{17}$$

where $\gamma = c_p/c_v$, with c_p is the constant-pressure specific heat. Equation 17 clearly simplifies to Eq. 11 when $\rho D/\eta = 1$. By solely using DMS transport data in Eq. 17, the kinetic theory result for κ (Eq. 17) is shown in Fig. 10a-b, where excellent agreement with the DMS computations is shown.

The analysis detailed here shows that (i) the Eucken approximation is reasonably accurate but can be improved with a refined evaluation of $\rho D/\eta$ for the gas under consideration, and (ii) the DMS transport data were found to be consistent with kinetic theory across a wide range of temperatures, thus lending further credibility to the methodologies employed for their determination.

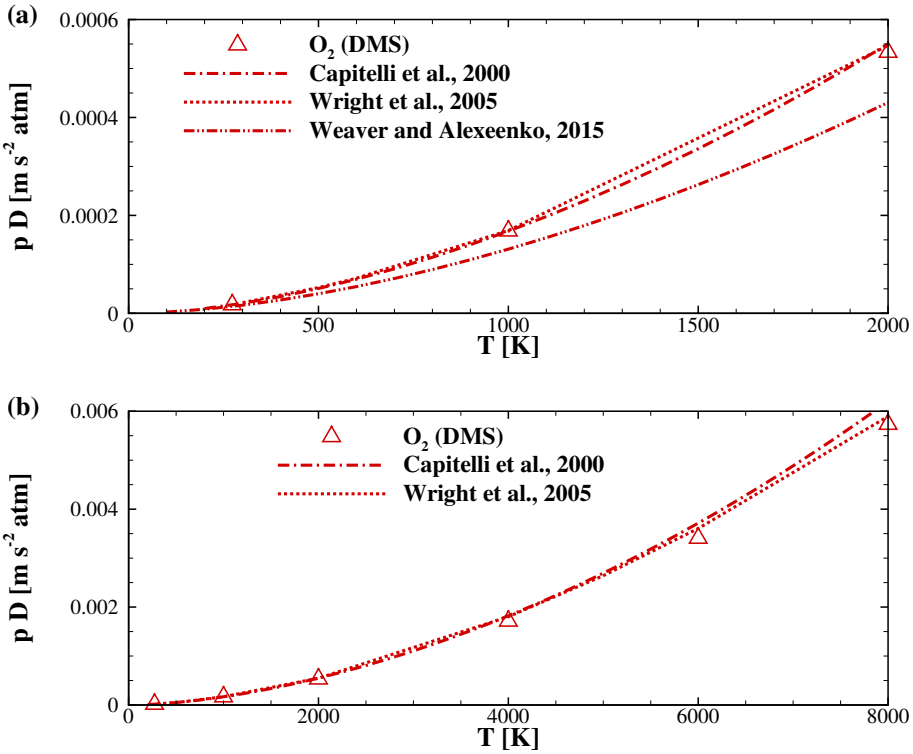

FIG. 8. Molecular oxygen self-diffusion coefficients from DMS and from transport collision integrals [30, 31, 51]: comparison at (a) low temperature and (b) over the entire temperature range considered in this work.

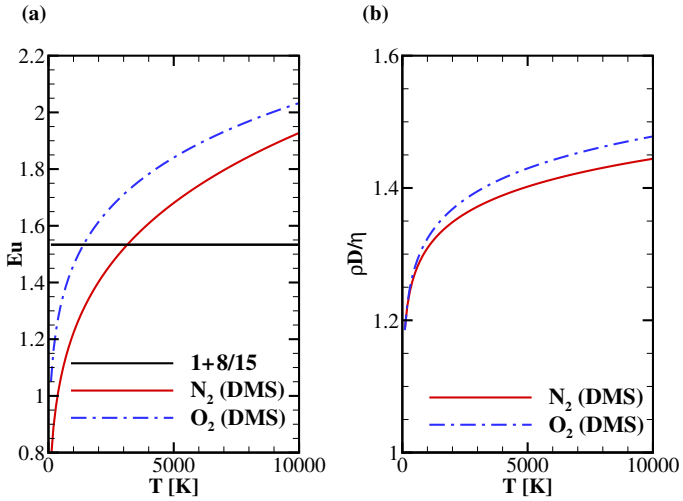

FIG. 9. (a) Temperature variation of the Eucken correction factor and (b) ratio of mass to momentum diffusion obtained from DMS transport data.

IV. CONCLUSIONS

The thermal conductivity and self-diffusion coefficients for molecular nitrogen and oxygen are investigated using the DMS technique based on sophisticated, *ab initio* PESs. For thermal conductivity, the DMS predictions are obtained by employing the MMP method, proposed by us in a recent study [16] and applicable to any stochastic particle method. The DMS results are

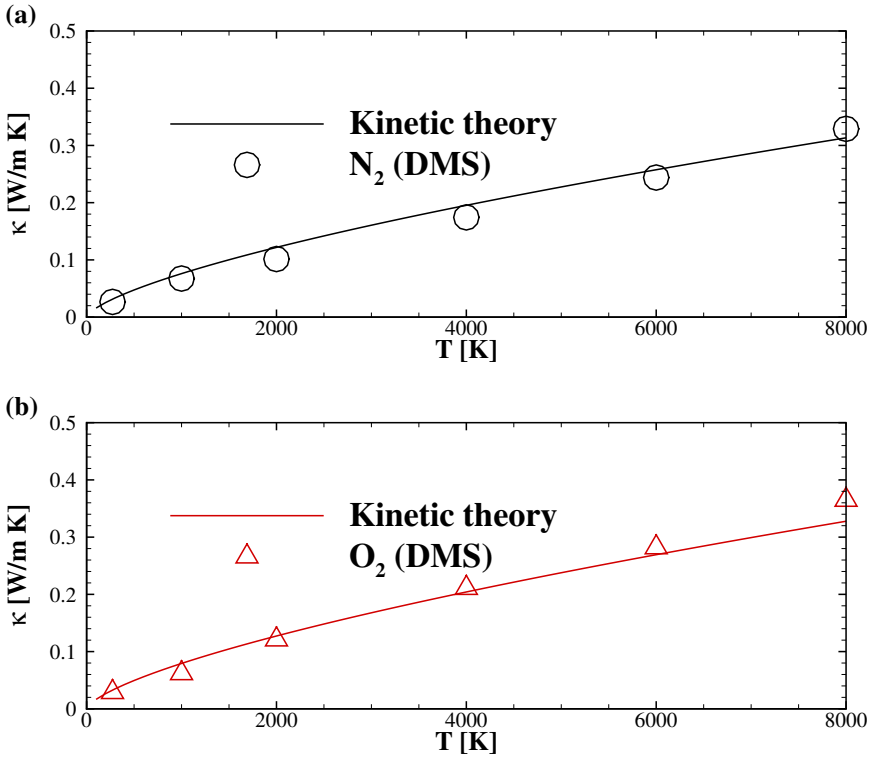

FIG. 10. Kinetic theory prediction for molecular thermal conductivity coefficient from DMS transport data for mass (D) and momentum (η) diffusion.

compared to experimental data at low temperatures (up to 2,000 K) and kinetic theory results up to 10,000 K. The DMS data agree remarkably well with the experimental data for both pure molecular nitrogen and oxygen. For a 22% O_2 and 78% N_2 by mole fraction, non-reacting mixture, the agreement with the experimental evidence is also very good [25]. The results obtained here for pure components are in very good accordance with the thermal conductivity coefficient obtained from collision integrals [30, 31], over a wide temperature range. At variance with simplified, point-particle potentials [33] used in the calculations of transport collision integrals, the *ab initio* PESs utilized in the simulations presented here are much more refined and account for the correct dimensionality of the molecular systems (i.e., 6-dimensional), without any low-temperature empirical input. In DMS, particles explicitly have all degrees of freedom corresponding to their chemical structure, and, thus, the effect of internal energy excitation is directly accounted for in the evaluation of transport coefficients (e.g., bond stretching at high temperature). Despite the difference in sophistication, there is very good agreement between the DMS data and the collision integral data [30, 31] up to about 10,000 K. For non-reactive air, we found that the DMS data for thermal conductivity agree well with the kinetic theory results of Gupta *et al.* [44] for equilibrium air at 1 atm, up to about 4,000 K. Beyond 4,000 K, the assumption of purely molecular composition (i.e., frozen composition) starts to break down, and the two data sets begin to diverge due to the formation of atomic species.

For mass self-diffusion, the DMS predictions are in very good accordance with the limited experimental evidence at near-room temperature [49, 50]. The results obtained here for molecular nitrogen and molecular oxygen are in excellent accordance with the self-diffusion data obtained from collision integrals [30, 31], over a wide temperature range. These detailed comparisons confirm the reliability of current high-temperature transport models recommended for use in popular thermochemical nonequilibrium CFD solvers [46].

An analysis of the Eucken approximation, conducted for pure components only, reveals that the Eucken correction is based upon reasonably accurate assumptions, but a significant improvement can be obtained by properly accounting for the ratio of mass to momentum diffusion. Furthermore, via this basic kinetic theory analysis, we show that the all DMS transport data (mass, momentum, and energy) were found to be consistent with kinetic theory across a wide range of temperatures, thus offering convincing evidence for the reliability of methodologies employed for their determination.

V. ACKNOWLEDGMENTS

The authors gratefully acknowledge funding from the Air Force Office of Scientific Research (AFOSR) through contract LRIR 21RQCOR045. Use of computational resources made available through the Department of Defense High Performance Computing Modernization Program (HPCMP) is greatly appreciated.

[1] J. J. D. Anderson, *Hypersonic and High-Temperature Gas Dynamics, AIAA Education Series, 2nd Ed.* (American Institute of Aeronautics and Astronautics, Inc., Reston, VA,, 2006).
[2] Y. Paukku, K. R. Yang, Z. Varga, and D. G. Truhlar, Global *ab initio* ground-state potential energy surface of N_4, J. Chem. Phys. **139**, 044309 (2013).
[3] J. D. Bender, P. Valentini, I. Nompelis, Y.Paukku, Z. Varga, D. G. Truhlar, T. E. Schwartzentruber, and G. V. Candler, An improved potential energy surface and multi-temperature quasiclassical trajectory calculations of N_2+N_2 dissociation reactions, J. Chem. Phys. **143**, 054304 (2015).
[4] Y. Paukku, K. R. Yang, Z. Varga, G. Song, J. D. Bender, and D. G. Truhlar, Potential energy surfaces of quintet and singlet O_4, J. Chem. Phys. **147**, 034301 (2017).
[5] Y. Paukku, Z. Varga, and D. G. Truhlar, Potential energy surface of triplet O_4, J. Chem. Phys. **148**, 124314 (2018).
[6] Z. Varga, Y. Paukku, and D. G. Truhlar, Potential energy surfaces for O+O_2 collisions, J. Chem. Phys. **147**, 154312 (2017).
[7] J. Li, Z. Varga, D. G. Truhlar, and H. Guo, Many-body permutationally invariant polynomial neural network potential energy surface for N4, J. Chem. Theory and Comput. **16**, 4822 (2020).
[8] Z. Varga, R. Meana-Pañeda, G. Song, Y. Paukku, and D. G. Truhlar, Potential energy surface of triplet N_2O_2, J. Chem. Phys. **144**, 024310 (2016).
[9] Z. Varga and D. G. Truhlar, Potential energy surface for high-energy N + N_2 collisions, Phys. Chem. Chem. Phys. **23**, 26273 (2021).
[10] W. Lin, Z. Varga, G. Song, Y. Paukku, and D. G. Truhlar, Global triplet potential energy surfaces for the $N_2(X^1\Sigma)$ + O(3p) $\rightarrow$ NO($X^2\prod$) + N(4S) reaction, J. Chem. Phys. **144**, 024309 (2016).
[11] P. Valentini, T. E. Schwartzentruber, J. D. Bender, I. Nompelis, and G. V. Candler, Direct molecular simulation of nitrogen dissociation based on an *ab initio* potential energy surface, Phys. Fluids **27**, 086102 (2015).
[12] P. Valentini, T. E. Schwartzentruber, J. D. Bender, and G. V. Candler, Dynamics of nitrogen dissociation from direct molecular simulation, Phys. Rev. Fluids **1**, 043402 (2016).
[13] M. S. Grover, T. E. Schwartzentruber, Z. Varga, and D. G. Truhlar, Vibrational energy transfer and collision-induced dissociation in O+O_2 collisions, J. Thermophys. Heat Tr. **33**, 797 (2019).
[14] M. S. Grover, E. Torres, and T. E. Schwartzentruber, Direct molecular simulation of internal energy relaxation and dissociation in oxygen, Phys. Fluids **31**, 076107 (2019).
[15] P. Valentini, A. M. Verhoff, M. S. Grover, and N. J. Bisek, First-principles predictions for shear viscosity of air components at high temperature, Phys. Chem. Chem. Phys. **25**, 9131 (2023).
[16] P. Valentini, M. S. Grover, N. J. Bisek, and A. M. Verhoff, *Ab initio* calculation of thermal conductivity: Application to molecular nitrogen, Phys. Rev. Fluids **7**, L071401 (2022).
[17] T. Mankodi, U. V. Bhandarka, and R. S. Myong, Collision cross sections and nonequilibrium viscosity coefficients of N_2 and O_2 based on molecular dynamics, Phys. Fluids **32**, 036102 (2020).
[18] E. Torres and T. E. Schwartzentruber, Direct molecular simulation of oxygen dissociation across normal shocks, Theor. Comp. Fluid Dyn. **36**, 1 (2022).
[19] M. S. Grover and P. Valentini, *Ab initio* simulation of hypersonic flows past a cylinder based on accurate potential energy surfaces, Phys. Fluids **33**, 051704 (2021).
[20] M. S. Grover, P. Valentini, T. E. Schwartzentruber, R. L. Jaffe, N. J. Bisek, and A. M. Verhoff, Comparative analysis of internal energy excitation and dissociation of nitrogen predicted by independently developed *ab initio* potential energy surfaces, Phys. Rev. Fluids **7**, 123401 (2022).
[21] P. Valentini, M. S. Grover, N. J. Bisek, and A. M. Verhoff, Molecular simulation of flows in thermochemical non-equilibrium around a cylinder using *ab initio* potential energy surfaces for N_2 + N and N_2 + N_2 interactions, Phys. Fluids **33**, 096108 (2021).
[22] R. S. Chaudhry and G. V. Candler, Statistical analyses of quasiclassical trajectory data for air dissociation, in *AIAA Scitech 2019 Forum*, https://arc.aiaa.org/doi/pdf/10.2514/6.2019-0789.
[23] P. Valentini, M. S. Grover, A. M. Verhoff, and N. J. Bisek, Near-continuum, hypersonic oxygen flow over a double cone simulated by direct simulation monte carlo informe from quantum chemistry, J. Fluid Mech. **966**, A32 (2023).
[24] W. A. Cole and W. A. Wakeham, The viscosity of nitrogen, oxygen, and their binary mixtures in the limit of zero density, J. Phys. Chem. Ref. Data **14** (1985).
[25] J. R. Lemmon, E.W., Viscosity and thermal conductivity equations for nitrogen, oxygen, argon, and air, Int. J. Thermophys. **25**, 21–69 (2004).
[26] S. Saxena and S. Chen, Thermal conductivity of nitrogen in the temperature range 350–2500 K, Mol. Phys. **29**, 1507 (1975).

[27] F. M. Faubert and G. S. Springer, Measurement of the thermal conductivity of argon, krypton, and nitrogen in the range 800–2000 K, J. Chem. Phys. **57**, 2333 (1972).

[28] P. W. Schreiber, A. M. Hunter, and K. R. Benedetto, Argon and nitrogen plasma viscosity measurements, Phys. Fluids **14**, 2696 (1971).

[29] M. S. Grover, A. M. Verhoff, P. Valentini, and N. J. Bisek, First principles simulation of reacting hypersonic flow over a blunt wedge, Physics of Fluids **35**, 086106 (2023).

[30] M. J. Wright, D. Bose, G. E. Palmer, and E. Levin, Recommended collision integrals for transport property computations, Part 1: air species, AIAA J. **43**, 2558 (2005).

[31] M. Capielli, C. Gorse, S. Longo, and D. Giordano, Collision integrals of high-temperature air species, J. Thermophys. Heat Trans. **14**, 259 (2000).

[32] M. Capitelli and R. S. Devoto, Transport coefficients of high-temperature nitrogen, Phys. Fluids **16**, 1835 (1973).

[33] A. B. Murphy and C. J. Arundell, Transport coefficients of argon, nitrogen, oxygen, argon-nitrogen, and argon-oxygen plasmas, Plasma Chem Plasma P. **14**, 451 (1994).

[34] J. O. Hirshfelder, C. F. Curtiss, and R. B. Bird, *Molecular Theory of Gases and Liquids, Structure of Matter Series* (John Wiley and Sons Inc., Hoboken, NJ, 1964).

[35] D. G. Truhlar and J. T. Muckerman, *Atom-Molecule Collision Theory: A Guide for the Experimentalist* (Plenum Press, New York, NY, 1979) p. 505.

[36] S. Subramaniam, R. L. Jaffe, and K. A. Stephani, State-resolved transport collision integrals for the O + O_2 system, Phys. Rev. Fluids **5**, 113402 (2020).

[37] T. E. Schwartzentruber, M. S. Grover, and P. Valentini, Direct molecular simulation of nonequilibrium dilute gases, J. Thermophysics Heat Tr. **32**, 892 (2018).

[38] G. A. Bird, *Molecular Gas Dynamics and Simulation of Gas Flows* (Cambridge University Press, Cambridge, England, 1994).

[39] E. Torres and T. E. Schwartzentruber, Direct molecular simulation of nitrogen dissociation under adiabatic postshock conditions, J. Thermophysics Heat Tr. **34**, 801 (2020).

[40] A. Y. K. Hong and M. A. Gallis, Optimized collision-specific parameters for binary mixtures of nitrogen, oxygen, argon, and helium, Physics of Fluids **35**, 10.1063/5.0157206 (2023), 061705.

[41] D. Frenkel and B. Smit, *Understanding Molecular Simulation: From Algorithms to Applications* (Academic Press, San Diego, CA, 2002).

[42] F. Müller-Plathe, A simple nonequilibrium molecular dynamics method for calculating the thermal conductivity, J. Chem. Phys. **106**, 6082 (1997).

[43] D. A. McQuarrie and J. D. Simon, *Physical Chemistry - A Molecular Approach* (University Science Books, Sausalito, California, 1997).

[44] R. N. Gupta, J. M. Yos, R. A. Thompson, and K.-P. Lee, *A review of reaction rates and thermodynamic and transport properties for an 11-species air model for chemical and thermal nonequilibrium calculations to 30,000 K*, Tech. Rep. 1232 (NASA, 2009).

[45] S. J. Farlow, *Partial differential equations for scientists and engineers* (Dover Publications, Inc., 1993).

[46] M. J. Wright, T. White, and N. Mangini, *Data Parallel Line Relaxation (DPLR) Code User Manual Acadia - Version 4.01.1*, NASA, Ames Research Center, Moffett Field, CA (2009).

[47] J. H. Ferziger and H. G. Kaper, *Mathematical theory of transport processes in gases* (North-Holland publishing company, 1993).

[48] A. Ern and V. Giovangigli, Thermal diffusion effects in hydrogen-air and methane-air flames, Combust. Theory Model. **2**, 349 (1998).

[49] E. B. Winn, The temperature dependence of the self-diffusion coefficients of argon, neon, nitrogen, oxygen, carbon dioxide, and methane, Phys. Rev. **80**, 1024 (1950).

[50] L. E. Boardman, N. E. Wild, and S. W. J. Smith, The diffusion of pairs of gases with molecules of equal mass, Proceedings of the Royal Society of London. Series A - Mathematical and Physical Sciences **162**, 511 (1937).

[51] A. B. Weaver and A. A. Alexeenko, Revised variable soft sphere and Lennard-Jones model parameters for eight common gases up to 2200 K, J. Phys. Chem. Ref. Data **44**, 023103 (2015).

[52] J. O. Hirschfelder, Heat conductivity in polyatomic or electronically excited gases. II, J. Chem. Phys. **26**, 282 (1957).